Ozone-Based Atomic Layer Deposition of Alumina from TMA: Growth, Morphology, and Reaction Mechanism

S. D. Elliott*

Tyndall National Institute, Lee Maltings, Cork, Ireland

G. Scarel, C. Wiemer, and M. Fanciulli

CNR-INFM MDM National Laboratory, Via C. Olivetti 2, 20041 Agrate Brianza, Italy

G. Pavia

STMicroelectronics, via C. Olivetti 2, 20041 Agrate Brianza, Italy

Received April 18, 2006. Revised Manuscript Received May 25, 2006

We examine the effect of growth temperature in the 150−300 °C range on the structural and morphological properties of Al_2O_3 films deposited using atomic layer deposition, contrasting the effect of H_2O and O_3 as oxygen sources. Trimethylaluminum (TMA) is the metal source. A mechanism for the O_3 reaction is investigated using ab initio calculations and provides an explanation for the observed temperature dependence. The simulations show that hydroxyl groups are produced at the surface by the oxidation of adsorbed methyl groups by O_3. This is confirmed by the measured rates; both H_2O and O_3 processes show molar growth rates per cycle that decrease with increasing reactor temperature, consistent with a decrease in hydroxyl coverage. At no temperature does the O_3 process deposit more Al_2O_3 per cycle than the H_2O process. Morphological characterization shows that O_3 as the oxygen source yields lower-quality films than H_2O; the films are less dense and rougher, especially at low growth temperatures. The existence of voids correlates with the low film electronic density. This may indicate the low mobility of surface hydroxyl at low temperatures, an effect that is washed out by repeated exchange with the vapor phase in the H_2O case.

1. Introduction

The atomic layer deposition (ALD) of alumina (Al_2O_3) using ozone (O_3) is studied over a wide temperature range and compared with the well-known H_2O process, focusing on the growth rate, film density, roughness, and reaction mechanism.

ALD is a type of chemical vapor deposition (CVD) in which precursors in gas form are admitted separately into the reactor in alternate pulses. Each precursor chemisorbs individually onto the substrate, rather than reacting in the gas phase.[1] Gas-phase reactions are avoided by purging with inert gas between each pulse. Under ideal conditions, substrate−precursor reactions are self-limiting and the surface is saturated with precursor fragments at the end of each pulse. Ligands in the fragments are eliminated by reaction with the other precursor during the next pulse. Because growth reactions occur only at the surface, deposition is slow, but with the advantage of atomic-level control of film thickness, as well as unparalleled conformality and uniformity. ALD is therefore used for the deposition of nanometer-thin films in high-aspect-ratio structures, such as alumina films in dynamic random access memory (DRAM) trenches,[2] read−write heads,[3] or in the interpoly dielectric stack of flash memories.[4]

The use of ozone (O_3) as oxygen precursor in metal-oxide ALD has stemmed from its higher activity for ligand elimination relative to H_2O. It is therefore needed for particularly stable metal (M) precursors, such as β-diketonates. For instance, Y_2O_3 has been deposited from yttrium β-diketonate and O_3,[5] and ZrO_2 has been deposited from various zirconium cyclopentadienyls and O_3[6] or H_2O.[7] It is interesting that both of these examples show temperature windows over which the growth rate is approximately constant. Another reason for a preference for O_3 is that H_2O adsorbs on reactor walls and is difficult to purge.

Along with these processing advantages, higher-quality film is sometimes produced by O_3 ALD when compared with H_2O. Much current research is directed toward the use of ALD of high permittivity films (e.g., ZrO_2,[7] HfO_2,[8,9,10] and Al_2O_3)[11,12,13] in the microelectronics industry. For the deposi-

* To whom correspondence should be addressed. E-mail: simon.elliott@tyndall.ie. Tel: 353-21-4904392. Fax: 353-21-4270271.

(1) Suntola, T. *Mater. Sci. Rep.* **1989**, *4*, 261−312.
(2) Ha, D.; Shin, D.; Koh, D. H.; Lee, J.; Lee, S.; Ahn, Y. S.; Jeong, H.; Chung, T.; Kim, K. *IEEE Trans. Electron Devices* **2000**, *47*, 1499.
(3) Paranjpe, A.; Gopinath, S.; Omstead, T.; Bubber, R. *J. Electrochem. Soc.* **2001**, *148*, G465−G471.
(4) Lee, T. P.; Jang, C.; Haselden, B.; Dong, M.; Park, S.; Bartholomew, L.; Chatham, H.; Senzaki, Y. *J. Vac. Sci. Technol., B.* **2004**, *22*, 2295−2298.
(5) Putkonen, M.; Sajavaara, T.; Johansson, L.-S.; Niinistö, L. *Chem. Vap. Deposition* **2001**, *7*, 44−50.
(6) Putkonen, M.; Niinistö, L. *J. Mater. Chem.* **2001**, *11*, 3141−3147.
(7) Niinistö, J.; Putkonen, M.; Niinistö, L.; Kukli, K.; Ritala, M.; Leskelä, M. *J. Appl. Phys*. **2004**, *95*, 84−91.
(8) Lee, S.-I.; Owyang, J. S.; Senzaki, Y.; Helms, A.; Kapkin, K. *Solid State Technol*. **2003**, *46*, 45−46.

10.1021/cm0608903 CCC: $33.50 © 2006 American Chemical Society
Published on Web 07/13/2006

tion of HfO_2, comparisons have been made between O_3 and H_2O, in combination with $HfCl_4$[8,9,10] or $Hf(NR_2)_4$ (R = Me, Et),[14] with pronounced temperature-dependence reported for the latter.[15] Most of the published reports indicate that, compared with films grown using H_2O as the oxygen source, the as-grown films deposited on Si using O_3 have a higher degree of crystallinity and[9] less incorporation of hydroxyl groups,[8,11] carbon,[13] and/or chlorine.[9] The deleterious SiO_2-like interfacial layer (IL) between the oxide and the Si substrate[8,12] was found to be thicker and of higher quality when investigated using X-ray photoelectron spectroscopy (XPS).[9,7] Moreover, the beginning of the growth process was found to be uninhibited and related to SiO_x layer formation during the first ALD cycles,[8,7,12] together with layer-by-layer rather than island type growth.[8,7] Finally, films deposited using O_3 as the oxygen source in general have better smoothness[9] (determined from atomic force microscopy (AFM)), less oxygen deficiency,[9,11,12] lower leakage currents due to better bulk and IL quality,[11] better chemical inertness,[11] less defects,[7] lower hysteresis and density of interface states after annealing in forming gas, close to that of the SiO_2/Si interface,[9,7] higher breakdown field strengths,[7] and smaller flat band voltage shift due to fixed charges, even though it is quite high compared to that of the SiO_2/Si interface.[9] Very recently, high-mobility substrates (such as Ge and GaAs) have gained increasing interest as alternatives to Si in microelectronics; on Ge, as-grown HfO_2 films deposited from $HfCl_4$ and O_3 are shown to be very promising from the point of view of the electrical properties.[10]

Similar results have been obtained for alumina ALD from trimethylaluminum (TMA), comparing O_3 with H_2O[11,16,17] and O_2 plasma;[17] even without postdeposition annealing, the O_3-prepared alumina films have a lower defect state density, lower leakage current, and smaller flatband voltage shift than the H_2O-prepared ones. One stated motivation for the use of O_3 is to minimize the formation of OH and related defect states.[11]

However, even though the properties of films deposited using O_3 are so promising, there are no systematic studies of the growth mechanisms and the properties of HfO_2, ZrO_2, and Al_2O_3 films deposited by ALD using O_3 as the oxygen source. This work therefore proposes a systematic study of a model metal-oxide film (Al_2O_3) deposited by ALD at various growth temperatures (T_g) using O_3 and compares them with films deposited in the same T_g range using H_2O as the oxygen source.

We choose Al_2O_3 as a model metal-oxide film system and TMA as a representative metal precursor. TMA shows the advantages of volatility and resistance to thermal decomposition (<370 °C). TMA + H_2O is a near-ideal ALD process that has been extensively studied, and the underlying reactions are well-understood,[18] especially on the basis of systematic measurements[19] and quantum mechanical calculations.[20,21]

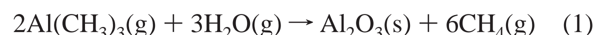

$$2Al(CH_3)_3(g) + 3H_2O(g) \rightarrow Al_2O_3(s) + 6CH_4(g) \quad (1)$$

Chemisorption of TMA and H_2O are Lewis acid−base reactions, whereas methyl ligands (CH_3^-) and hydroxyl protons (H^+) combine in a Brønsted acid−base reaction and are eliminated as methane during both TMA and H_2O pulses.

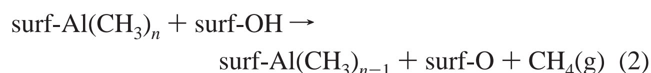

$$\text{surf-Al}(CH_3)_n + \text{surf-OH} \rightarrow \text{surf-Al}(CH_3)_{n-1} + \text{surf-O} + CH_4(g) \quad (2)$$

Oxidation is a more-energetic alternative to using H_2O to remove ligands from the surface, but little is known about the chemistry underlying this process. No systematic study has yet been carried out on the temperature dependence of the growth rate for TMA + O_3, and there is no unanimous view on the subject. J. Kim et al.[22] report that the growth rate increases with increasing T_g for O_3 (especially beyond 350 °C) but that the opposite occurs using H_2O.[19] On the other hand, S. K. Kim and Hwang,[12] working at T_g = 400 °C, noticed that films were deposited using H_2O at a higher rate than those using O_3. An important clue is obtained from time-of-flight secondary ion mass spectrometry (TOF-SIMS),[13] which shows that the H concentration within the film and at the surface is similar for both H_2O and O_3 processes (whereas the C% is lower in the latter); it is therefore probable that the reactions of the TMA pulse proceed identically for both processes, with the evolution of CH_4. However, in other work, C_2H_6 is proposed as the only byproduct of the reaction.[11]

The mechanism of the TMA + O_3 process is poorly understood compared to that of TMA + H_2O. It is reasonable to assume that O_3 decomposes into O_2 and monatomic O, and that the latter is the active species. The efficiency of O_3 decomposition[23] is ambient- and temperature-dependent: the half-life of O_3 in air is 1.5 h at 120 °C and 1.5 s at 250 °C; the half-life in water is already 8 min at 35 °C. It is likely that the O radical breaks apart ligand fragments on the surface, which desorb once a volatile product is formed. The most-frequent assumption is that O_3 burns off organic ligands

(9) Park, H. B.; Cho, M.; Park, J.; Lee, S. W.; Hwang, C. S.; Kim, J.-P.; Lee, J.-H.; Lee, N.-I.; Kang, H.-K.; Lee, J.-C.; Oh, S.-J. *J. Appl. Phys.* **2003**, *94*, 3641−3647.
(10) Spiga, S.; Wiemer, C.; Tallarida, G.; Scarel, G.; Ferrari, S.; Seguini, G.; Fanciulli, M. *Appl. Phys. Lett*. **2005**, *87*, 112904.
(11) Kim, J. B.; Kwon, D. R.; Chakrabarti, K.; Lee, C.; Oh, K. Y.; Lee, J. H. *J. Appl. Phys.* **2002**, *92*, 6739−6742.
(12) Kim, S. K.; Hwang, C. S. *J. Appl. Phys.* **2004**, *96*, 2323−2329.
(13) Jakschik, S.; Schroeder, U.; Hecht, T.; Krueger, D.; Dollinger, G.; Bergmaier, A.; Luhmann, C.; Bartha, J. W. *Appl. Surf. Sci.* **2003**, *211*, 352−359.
(14) Cho, M. J.; Jeong, D. S.; Park, J.; Park, H. B.; Lee, S. W.; Park, T. J.; Hwang, C. S.; Jang, G. H.; Jeong, J. *Appl. Phys. Lett.* **2004**, *85*, 5953−5955.
(15) Kamiyama, S.; Miura, T.; Nara, Y. *Appl. Phys. Lett.* **2005**, *87*, 132904.
(16) Ha, S.-C.; Choi, E.; Kim, S.-H.; Roh, J. S. *Thin Solid Films* **2005**, *476*, 252−257.
(17) Cho, M.; Park, H. B.; Park, J.; Lee, S. W.; Hwang, C. S.; Jeong, J.; Kang, H. S.; Kim, Y. W. *J. Electrochem. Soc.* **2005**, *152*, F49−F53. Kim, S. K.; Lee, S. W.; Hwang, C. S.; Min, Y. S.; Won, J. Y.; Jeong, J. *J. Electrochem. Soc.* **2006**, *153*, F69−F76.
(18) Puurunen, R. L. *J. Appl. Phys.* **2005**, *97*, 121301.
(19) Matero, R.; Rahtu, A.; Ritala, M.; Leskelä, M.; Sajavaara, T. *Thin Solid Films* **2000**, *368*, 1−7.
(20) Elliott, S. D.; Greer, J. C. *J. Mater. Chem.* **2004**, *14*, 3246−3250.
(21) Heyman, A.; Musgrave, C. B. *J. Phys. Chem. B* **2004**, *108*, 5718−5725.
(22) Kim, J.; Chakrabarti, K.; Lee, J.; Oh, K.-Y.; Lee, C. *Mater. Chem. Phys.* **2003**, *78*, 733−738.
(23) Wulf, O. R. The Thermal Decomposition of Ozone. Ph.D. Thesis, California Institute of Technology, Pasadena, CA, 1926; http://etd.caltech.edu/etd/available/etd-11042004−153821/.

Table 1. Thickness, Electronic Density, Growth Rate, and Roughness of Al_2O_3 Films Resulting from the XRR Data Fitting

film code	T_g (°C)	oxygen source	duration of oxygen precursor pulse (s)	thickness[a] after 212 cycles (nm)	electronic density[b] ($e^-/Å^3$)	normalized growth rate (Al_2O_3/nm^2 per cycle)	rms roughness[c] (nm)
a	150	H_2O	3	23.9	0.97	1.76 ± 0.10	0.4
b	150	O_3	6	28.5	0.79	1.52 ± 0.09	0.7
c	200	H_2O	3	23.6	0.95	2.06 ± 0.11	0.5
d	200	O_3	6	22.2	0.87	1.90 ± 0.12	0.7
e	250	H_2O	3	22.3	0.98	2.11 ± 0.12	0.8
f	250	O_3	6	23.2	0.87	1.82 ± 0.11	1.1
g	300	H_2O	3	20.3	0.92	2.19 ± 0.12	0.6
h	300	O_3	6	17.5	0.92	2.12 ± 0.14	0.8

[a] Error in thickness is ±0.1 nm. [b] Error in the electronic density is ±0.05 $e^-/Å^3$. [c] Error in thickness is ±0.1 nm.

to CO_2 and H_2O.[24] To form H_2O, the hydride anion H^- must be stripped from the CH_3 ligand during its oxidation by O_3. To form CO_2, successive oxygen atoms must attack the C center directly before it desorbs from the surface.

However, CO_2 and H_2O are not the only volatile products that can result from oxidation of the CH_3 ligand. A potential mechanism for TMA + O_3 has been reported on the basis of ab initio cluster calculations of the insertion of O into the Al−C bond, followed by ethene (C_2H_4) desorption.[25]

$$\text{surf-Al(CH}_3)_n + \text{O}_3\text{(g)} \rightarrow \text{surf-Al(CH}_3)_{n-1} + \text{surf-OH} + {}^1/_2\text{C}_2\text{H}_4\text{(g)} + \text{O}_2\text{(g)} \quad (3)$$

This mechanism yields surface OH as a product of the O_3 pulse, so that protons are available for the elimination of CH_4 during the TMA pulse (eq 2), as in the case of TMA + H_2O ALD. Here, we carry out calculations on reactants, intermediates, and products of eq 3.

Such a mechanism contradicts previous assumptions that the O_3 process minimizes the production of OH and related defect states.[11] In fact, if enough surface OH is produced, it may also be important to consider H_2O as a product. At temperatures where diffusion is sufficiently high, surface hydroxyl can associate into H_2O and desorb

$$\text{surf-OH} + \text{surf-OH} \rightarrow \text{surf-O} + \text{H}_2\text{O(g)} \quad (4)$$

and so excess OH is likely to be lost during the oxygen precursor pulse and subsequent purge, until the equilibrium OH coverage is achieved.

In this way, combining calculations on the growth mechanism and experiments regarding the effects of T_g (150−300 °C) on the properties of films deposited using O_3 as the oxygen source, we aim to provide an understanding of the growth process and film morphology in terms of a chemical mechanism for deposition. We directly compare alumina films deposited using H_2O and O_3 as the oxygen sources under similar experimental conditions (T_g, number of cycles, cycle length) and use first-principles density functional theory (DFT) calculations to investigate the reaction mechanism and its impact on growth rate and morphology.

In the first part of the paper, the experiments are described, including growth parameters, substrate preparation, and structural analysis. The experimental results on alumina film characterization are then reported. In the second part of the paper, the computational methods and models are described, followed by results of modeling of the growth of alumina films using TMA and either H_2O or O_3 as the oxygen source. The third section then discusses how the experimental and theoretical data can be synthesized into a picture of O_3 ALD.

2. Experimental Section

2.1. Film growth by ALD. The Al_2O_3 films were deposited by ALD in a flow type F-120 ASM Microchemistry Ltd. reactor. The films were grown on H-terminated Si(100). The hydrophobic Si surfaces were obtained after RCA (Radio Corporation of America) cleaning (HCl:H_2O_2:H_2O = 1:1:5 ratio, 10 min at 85 °C) followed by a 30 s rinse in deionized water and a 30 s dip in a dilute HF solution (HF:H_2O = 1:50) at room temperature. The ALD cycle consisted of (a) TMA-precursor injection (1 s); (b) N_2 purge (3 s); (c) oxygen-precursor injection (3 s for H_2O and 6 s for O_3); and (d) N_2 purge (2 s after the H_2O pulse, 4 s after the O_3 pulse). Note that the O_3 pulse is always longer than the H_2O one. For all the films, 212 ALD cycles were applied. T_g was chosen at 150 °C (films a and b), 200 °C (c, d), 250 °C (e, f) and 300 °C (g, h). A low and equal H_2O dose regime was applied in all depositions using H_2O. O_3 was injected into the reactor in a flux ≤390 sccm at a concentration of 160−170 g/Nm^3. We experimentally observed that, at this concentration of O_3 in the N_2/O_3 gas mixture introduced into the reactor, the same film growth rate for the same kind of oxide deposited using H_2O or O_3 was obtained when the pulse time for the latter was higher than the one for the former. The main film characteristics are summarized in Table 1.

2.2. XRR and TEM/ESI Characterization. Film layer thickness was determined using X-ray reflectivity (XRR) on pieces that were placed in the same position in the F-120 reactor during all depositions. The XRR data are acquired with the Italstructures HRD 3000 system with an angular step of 0.01° in the incidence angle. The data are shown in Figure 1. A low-density cap layer on the top of the Al_2O_3 layer was always necessary to correctly simulate the experimental data. The Al_2O_3 layer thickness, electronic density, and root-mean-square (rms) surface roughness are reported in Table 1. The normalized growth rate reported in Table 1 is obtained by converting the electronic density to molar density (50 electrons per Al_2O_3) and then by multiplying it by the thickness increment per cycle.

For the films deposited at the lowest T_g, i.e., films a and b, the cross section image was observed using transmission electron microscopy (TEM). The microscope used is a TECNAI F30 equipped with an energy filter. Bright field images were acquired using only elastically scattered electrons, thus overcoming chromatic aberration effects of the TEM lenses. Compositional maps were acquired using three-window electron spectroscopy imaging (ESI).

(24) Puurunen, R. L. *Chem. Vap. Deposition* **2003**, *9*, 327−332.
(25) Prechtl, G.; Kersch, A.; Schulze Icking-Konert, G.; Jacobs, W.; Hecht, T.; Boubekeur, H.; Schroeder, U. *Tech. Dig.−Int. Electron Devices Meet.* **2003**, 245−248.

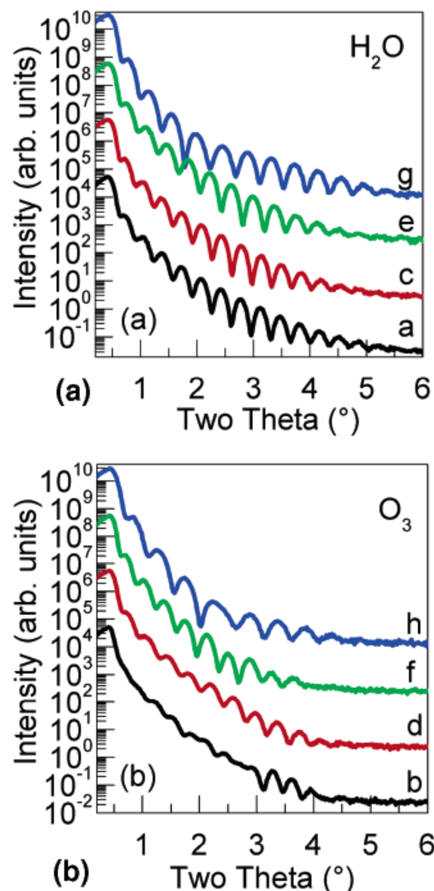

Figure 1. XRR spectra of films grown (top) using H_2O as the oxygen source at (a) 150, (c) 200, (e) 250, and (g) 300 °C, and (bottom) using O_3 as the oxygen source at (b) 150, (d) 200, (f) 250, and (h) 300 °C.

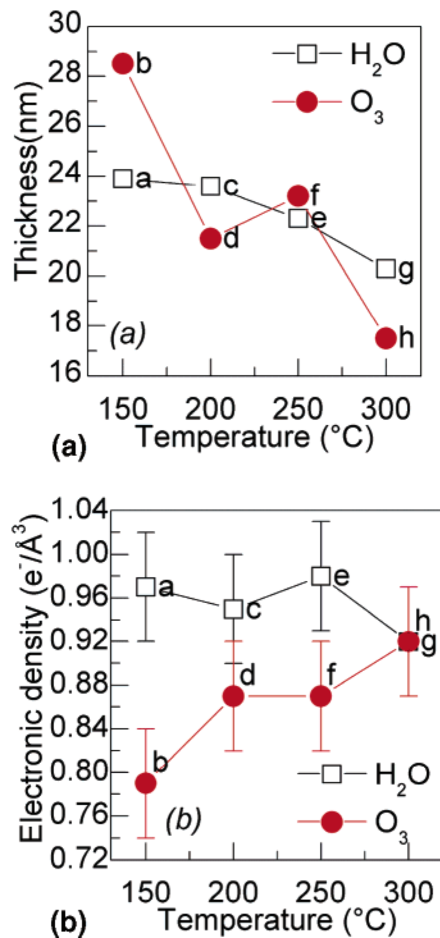

Figure 2. (a) Thickness (212 cycles of ALD) and (b) electronic density vs T_g for films grown using H_2O (open squares) and O_3 (dots) as the oxygen sources (Table 1).

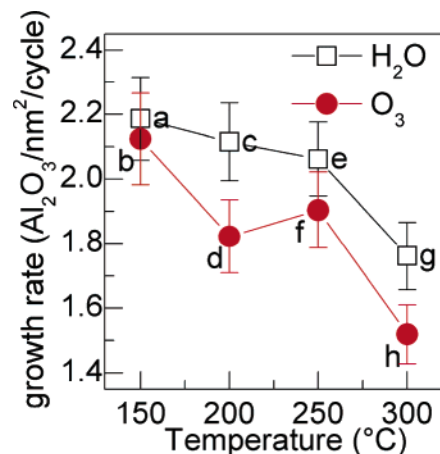

Figure 3. Variation of normalized growth rate (Table 1) with temperature for Al_2O_3 ALD using H_2O (open squares) and O_3 (dots) as the oxygen sources.

Failure to prepare film a for TEM analysis via polishing plus dimpler followed by Ar ion mill indicated this film had very poor adhesion on H-terminated Si(100). Dual-beam preparation was therefore applied to avoid using glues that might strip away the film from the substrate. No adhesion problems were revealed for film b, deposited at 150 °C using O_3 as the oxygen source.

2.3. Results. Film thickness values of films a−h deposited at T_g = 150−300 °C are summarized in Table 1 and Figure 2a. There is clearly a dependence of the thickness increment per cycle on both T_g and on the type of oxygen source (H_2O or O_3). For H_2O, the thickness of film deposited decreases slightly as T_g is raised, as is well-known.[18,19] With O_3 as the oxygen source, however, the decrease in thickness with T_g is more significant. For instance, film b, deposited using O_3 at T_g = 150 °C, is 20% thicker than the comparable H_2O-derived film a, whereas film h, deposited using O_3 at T_g = 300 °C, is 15% thinner than film g.

The electronic density data of the Al_2O_3 films are also summarized in Table 1 and Figure 2b. Films deposited using H_2O as the oxygen source exhibit an almost-constant electronic density (0.92−0.98 $e^-/Å^3$) across the range of T_g. This value is consistent with the electronic density of an amorphous film, which is lower than that of bulk sapphire (1.186 $e^-/Å^3$)[26] and is in agreement with previous ALD results for as-grown (amorphous) alumina films.[27]

For the O_3 process, we find that densities similar to those of films grown with H_2O are achieved only at high T_g (300 °C). At low T_g, the use of O_3 leads to films with much lower electronic density (0.79 $e^-/Å^3$ at 150 °C).

Combining the thickness and density data, we see that ALD with O_3 at low T_g yields a thick but low-density film (b) when compared to that with H_2O (a). We therefore calculate the normalized growth rate, expressing the amount of Al_2O_3 product deposited per ALD cycle (Table 1 and Figure 3). This shows that for both processes, the growth rate decreases with T_g but that the effect is more marked

(26) File 30024 for the corundum phase, File 68771 for the gamma phase, and File 66558 for $Al_{2.144}O_{3.20}$. *Inorganic Crystal Structure Database*; Fachinformationszentrum Karlsruhe: Karlsruhe, Germany, 2005.

(27) Scarel, G.; Wiemer, C.; Spiga, S.; Tallarida, G.; Evangelou, E. K.; Ferrari, S.; Fanciulli, M.; Zenkevich, A.; Lebedinskii, Y. *Comparison of Al_2O_3 Films Grown by Atomic Layer Deposition and Reactive Sputtering*. Presented at the 2002 MRS Fall Meeting, Boston, Dec 2−6, 2002.

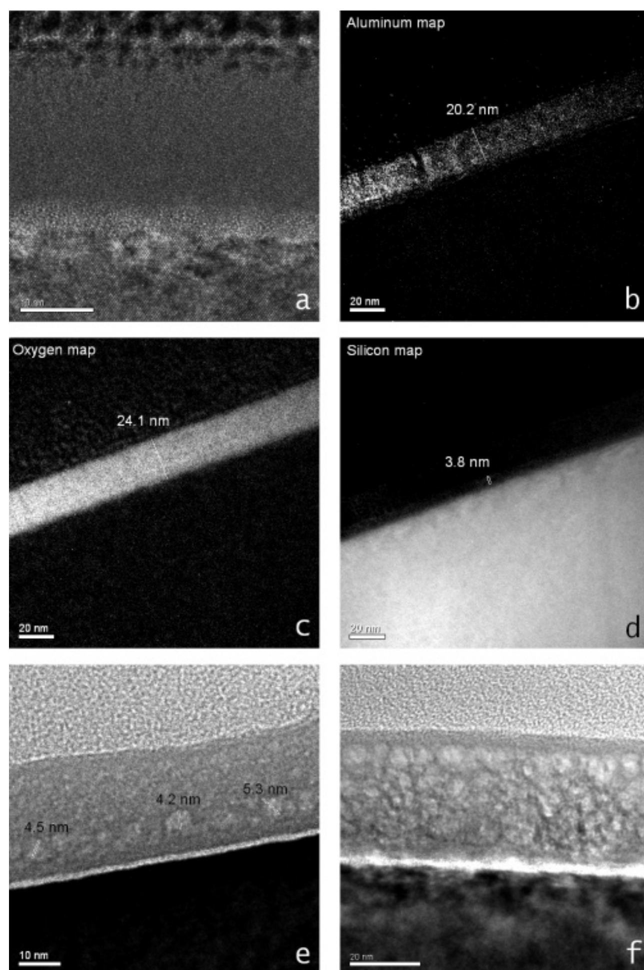

Figure 4. (a) TEM image ,and ESI of (b) aluminum, (c) oxygen, and (d) silicon maps of film a (150 °C, H_2O). (e) TEM image and (f) unfocused TEM image of film b (150 °C, O_3).

for O_3 than H_2O. The highest deposition rate is at low temperature (2.1−2.2 Al_2O_3/nm^2/cycle at 150 °C), approximately the same whether using O_3 or H_2O. As T_g is raised, O_3 produces progressively less Al_2O_3 per cycle than H_2O; for example, at 300 °C, the O_3 process is 15% slower.[28]

To investigate the nature of the low-density films deposited at $T_g = 150$ °C with various oxygen sources, we compared joint TEM analysis and ESI elemental mapping of films a and b (Figure 4). Film a, deposited using H_2O, is a uniform and compact amorphous film without holes (Figure 4a). Right above the Si substrate, a layer of light gray color, about 2.5−3 nm thick, can clearly be seen. The average thickness of the whole film measured from the TEM micrographs is about 23−25 nm. ESI maps of film a (Figure 4b−d) reveal that Al and O are uniformly distributed in the Al_2O_3 layer. However, the Al and O layers do not have the same thickness; the former is 20.2 nm, the latter 24.1 nm. The difference in thickness of the O and Al layers is 3.9 nm, which correlates well with the 3.8 nm light-gray layer above the Si substrate appearing in the Si layer (Figure 4d). Whereas the O layer (Figure 4c) is uniform across its overall thickness, the Al layer (Figure 4b) looks denser in its upper region than in its bottom one. Careful examination of the ESI images reveals that the light-gray layer on top of Si is richer in O than in all other elements (especially Si and Al) and, although we cannot quantify the stoichiometry of the layer, it is certainly

(28) The combination of both O_3 and H_2O only partially recovers the growth rate of the films with H_2O alone as the oxygen source; data are not presented here.

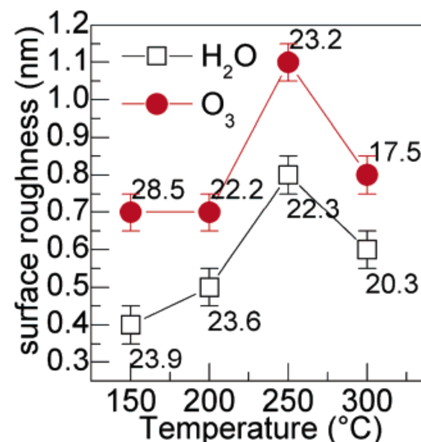

Figure 5. Roughness vs T_g for films grown using H_2O (open squares) and O_3 (dots) as the oxygen source (Table 1). The thickness (nm) of each sample (see Figure 2) is used to label the data.

oxygen-rich compared to expected compounds such as SiO_2 and Al_2O_3. The identity of this 3.8−3.9 nm thick oxygen-rich IL thus remains an open question.

On the other hand, the film deposited using O_3 at $T_g = 150$ °C (film b) is ~26 nm thick according to TEM analysis and exhibits a thin IL about 1.2 nm thick, as expected. Uniformly distributed in the film layer are round, clear-gray areas, 4.2−5.3 nm in diameter, clearly visible in Figure 4e. These areas correspond to either voids or lower-density regions, which account for the overall low density measured on this film. The voids can be even better identified in the out-of-focus image (Figure 4f). ESI maps (not shown) reveal the voids to contain less oxygen than the surrounding film and so they might be mostly empty. TOF-SIMS data (not shown) indicate that the carbon signal in film b is 2 orders of magnitude higher than that of film g (note, for comparison, that in film a, the carbon signal is only 1 order of magnitude higher than in film g). Given that carbon in film b is, however, below the detection limit of ESI, we can assume its amount in the film to be less than a few percent. Moreover, there is no carbon contamination at the interfacial layer (IL) with the Si substrate. On the other hand, TOF-SIMS of films a and g reveal that a small amount of carbon, again less than a few percent, exists at the IL. Low densities are found in films deposited at $T_g \leq 200$ °C using ALD and O_3 as the oxygen source in other cases as well, e.g., HfO_2[29] and NiO.[30] (We measured the electronic density for HfO_2 films deposited from $HfCl_4$ and O_3 at $T_g = 200$ and 350 °C to be 1.57 and 2.56 $e^-/Å^3$, respectively).

The rms surface roughness values of the Al_2O_3 films a−h measured using XRR are summarized in Table 1 and Figure 5. It is worth noticing that the XRR-determined rms surface roughness differs from the one measured using AFM because it takes into account not only the physical roughness but also the electronic density variations at the film/air interface.[31] However, the trends determined using both techniques are similar. The XRR measured rms surface roughness values of film a, deposited at 150 °C and using H_2O as the oxygen source, are equal to the values measured using AFM on Al_2O_3 films deposited at 33 and 177 °C also using H_2O.[32] From the data reported in Table 1 and Figure 5, it is observed that the Al_2O_3 films deposited using O_3 are slightly rougher than those deposited using H_2O as the oxygen source. The surface roughness values for O_3 vary in the 0.7−1.0 nm range, whereas

(29) Scarel, G.; et al. Unpublished.
(30) Scarel, G.; Li, X.; Wiemer, C.; Fanciulli, M. Unpublished.
(31) Van der Lee, A.; Durand, J.; Blin, D.; Holliger, Ph.; Martin, F. *Eur. Phys. J. B* **2004**, *39*, 273−277.
(32) Groner, M. D.; Fabreguette, F. H.; Elam, J. W.; George, S. M. *Chem. Mater*. **2004**, *16*, 639.

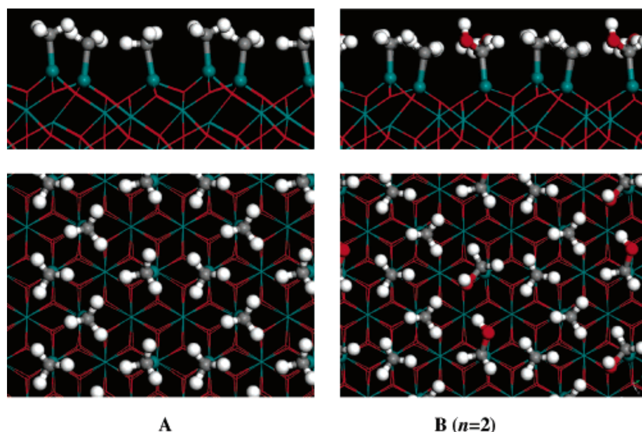

Figure 6. Side (top panel) and top (bottom panel) views of 2 × 2 surface models during oxidation with ozone. Left: initial methylated surface (**A**) $Al_2(CH_3)_6$. Right: reaction intermediate (**B**) $Al_2(CH_3)_4(CH_2OH)_2$. Red = O, blue/green = Al, gray = C, and white = H; lines indicate the α-Al_2O_3-(0001) substrate; balls show the surface atoms.

the values for the films deposited using H_2O vary in range 0.4−0.8 nm. The peak in surface roughness for deposition at T_g = 250 °C (films e and f) is not yet understood.

3. Computational

3.1. Methods and Models. The first-principles method is established as a reliable way to compute the bulk and surface properties of materials, especially their atomic structure and reaction energetics.[33] Self-consistent DFT within 3D, periodic boundary conditions is used to compute the ground-state electronic structure and total energy. Within these boundary conditions, the surface is modeled by an infinite series of stacked crystalline slabs, separated by vacuum. We employ the VASP package,[34,35,36] ultrasoft pseudo-potentials,[37,38] the PW91 density functional,[39] and a standard set of technical parameters.[40]

A six-layer (13 Å) slab of α-Al_2O_3 is used as the substrate to simulate a growing alumina film, with a vacuum of 12 Å between slab faces, as detailed previously.[20] The top face of the slab is decorated with adsorbed methyl groups (CH_3) to simulate the saturated surface that obtains at the start of the O_3 pulse. The bottom face of the slab is bare and remains unreconstructed when relaxed during the redox reactions of the top face. A 2 × 2 surface cell[41] is generated in order to minimize intercell image interactions and to maximize relaxation of adsorbate. During optimization, all ions are free to move within this fixed lattice. The methylated slab is $Al_{50}O_{72}C_6H_{18}$ = $(Al_2O_3)_{24}Al_2(CH_3)_6$ and is denoted A (Figure 6). This corresponds to a surface CH_3 coverage of θ(C) = 7.5 CH_3/nm^2 = 12.5 μmol/m^2, which matches a previous theoretical estimate made on the basis of van der Waals radii (7.2 CH_3/nm^2)[24] and is higher than typical experimental values[18] of 5−6 CH_3/nm^2. Reference energies of gas-phase atoms and molecules were computed within a cubic cell of side 15 Å.

To model a rational series of oxidized systems that may occur during the O_3 pulse, we investigate the reactions that can occur between surface **A** and successive singlet O atoms. Such O atoms may come from the thermal or photolytic dissociation of O_3 or O_2 or from an oxygen plasma, but there are well-known deficiencies in the DFT treatment of these molecules,[42,43] so we use singlet O(^{1}D) as the reference reactant throughout. In any case, we base our arguments on the relative energies of products, which are unaffected by the choice of reactant. No transition states or activation energies are computed. A complete consideration of spin states other than the non-spin-polarized singlet is beyond the scope of the current work.

3.2. Results. We initially investigated the reaction channels for O(^{1}D) with the methylated surface by carrying out short molecular dynamics runs on the DFT potential-energy hypersurface.[44] Abstraction by O of H^- from a CH_3 group is observed within 100 fs, and a variety of products are suggested by the subsequent dynamics, although the simulations are too short to reveal the final products of O_3 treatment. Motivated by these results, we postulate a reaction pathway for the O_3 ALD pulse (eq 3). We use DFT to optimize the geometries obtained by MD, giving intermediates along this pathway and their relative energetics (Table 2). To facilitate direct comparison, we carried out each series of calculations with the same number of oxidizing O atoms per unit cell (n). The consistency of ΔE per O across different n in Table 2 indicates that the approach is reliable. If hydroxyl groups are generated at the surface by the O_3 pulse, it is safe to assume that the subsequent TMA pulse proceeds as in the TMA + H_2O process.

The central assumption of this reaction pathway is that oxidation occurs uniformly across the surface and that elimination reactions follow before more O can react at a given C center. Attack by a single O on the CH_3 groups of model A produces surface CH_2OH, which is labeled B and shown in Figure 6. The surface C atom is oxidized in the reaction A → B; this oxidative adsorption step is computed to be highly exoergic. (The actual DFT value of −550 kJ/mol per O(^{1}D) may not be reliable, as noted above). An alternative geometry, in which both CH_2 and OH bind directly to Al, was found to be unstable, and a pair of adjacent CH_2 can combine to produce ethene (C_2H_4) via a triplet transition state (not shown here). Desorption of C_2H_4 reduces the surface and leaves surface OH (C, Figure 7). This elimination reaction B → C is computed to be exoergic by 150−190 kJ/mol per O (Table 2). The reaction pathway is efficient insofar as each oxidizing O eliminates one C from the surface and produces one OH group. We note that the metal ion (Al^{3+}) is neither oxidized nor reduced during these reactions.

Alternatively, O may insert into the Al−C bond to yield a methoxy ligand (Al−O−CH_3, D, Figure 7), as proposed by Prechtl et al.[25] D and C are computed to be approximately isoenergetic, probably because of Al−O formation in both cases. However, we find no evidence for a reaction path to link D and C, so that D may function as an O trap, preventing the elimination reaction.

We have computed some alternative reaction pathways, where more than one O reacts with each C center before desorption of

(33) Payne, M. C.; Teter, M. P.; Allan, D. C.; Arias, T. A.; Joannopoulos, J. D. *Rev. Mod. Phys.* **1992**, *64*, 1045−1097.
(34) Kresse, G.; Hafner, J. *Phys. Rev. B* **1994**, *49*, 14251−14269.
(35) Kresse, G.; Furthmüller, J. *Phys. Rev. B* **1996**, *54*, 11169−11176.
(36) Kresse, G.; Furthmüller, J. *Comput. Mater. Sci.* **1996**, *6*, 15−50.
(37) Vanderbilt, D. *Phys. Rev. B* **1990**, *41*, 7892−7895.
(38) Kresse, G.; Hafner, J. *J. Phys.: Condens. Matter* **1994**, *6*, 8245−8257.
(39) Perdew, J. P.; Chevary, J. A.; Vosko, S. H.; Jackson, K. A.; Pederson, M. R.; Singh, D. J.; Fiolhais, C. *Phys. Rev. B* **1992**, *46*, 6671−6687.
(40) We found that it was sufficient to use the Γ point only, because the cell was large and the system was insulating. The plane wave cutoff was 396 eV. Self-consistent steps were converged to 1 × 10^{-4} eV, and optimization of the ionic geometry was carried out until gradients were <1 × 10^{-3} eV/Å.
(41) The simulation cell is defined by lattice vectors a = (8.315x, −4.801y, 0z) Å, b = (8.315x, 4.801y, 0z) Å, c = (0x, 0y, 26.196z) Å.
(42) Stampfl, C.; Scheffler, M. *Phys Rev. B* **1996**, *54*, 2868−2872.
(43) Yoshioka, Y.; Yamaki, D.; Kubo, S.; Nishino, M.; Yamaguchi, K.; Mizuno, K.; Saito, I. *Electron. J. Theor. Chem.* **1997**, *2*, 236−252.
(44) Simulation parameters for MD runs: 500 steps of molecular dynamics were carried out with Δt = 0.5 fs using a Verlet algorithm with no fixed atoms and no constraints (i.e., microcanonical ensemble). The starting geometry consisted of one O atom per cell, 2 Å above the topmost H of the methylated surface ($Al_{25}O_{37}C_3H_9$ cell), and velocities corresponding to T = 500 K were assigned randomly.

Table 2. DFT Energetics for Oxidation of a Methylated Surface by O Atoms during the O_3 Pulse

	surface formula per 2 × 2 slab[b]	relative energy[a] per slab, ΔE (kJ/mol)			relative energy[a] per O, $\Delta E/n$ (kJ/mol of O)			
		$n = 1$	$n = 2$	$n = 4$	$n = 1$	$n = 2$	$n = 4$	
A	$Al_2(CH_3)_6 + n{\cdot}O(^1D)(g)$	+704	+1431	+2916	+704	+716	+729	Figure 6
B	$Al_2(CH_3)_{6-n}(CH_2OH)_n$	+149	+324	+759	+149	+162	+190	Figure 6
C	$Al_2(CH_3)_{6-n}(OH)_n + n/2{\cdot}C_2H_4(g)$	0	0	0	0	0	0	Figure 7
D	$Al_2(CH_3)_{6-n}(OCH_3)_n$	+2.2	+19.9	+40.1	+2.2	+9.9	+10.6	Figure 7
E	$Al_2(CH_3)_{6-n/4}(OH)_{n/4} + n/4{\cdot}CO_2(g) + n/4{\cdot}H_2O(g)$	n/a[c]	n/a[c]	+255	n/a[c]	n/a[c]	+63.6	
F	$Al_2(CH_3)_{6-n}O_{n/2} + n/2{\cdot}C_2H_4(g) + n/2{\cdot}H_2O(g)$	n/a[c]	+139	+386	n/a[c]	+69.5	+96.5	

[a] Energies are quoted relative to the most stable surface (C) for the whole system and scaled by the number of oxidizing O atoms (n). There is no correction for zero-point energy. [b] The 2 × 2 slab consists of an $(Al_2O_3)_{48}$ substrate as well as the listed surface atoms. [c] n/a = not applicable.

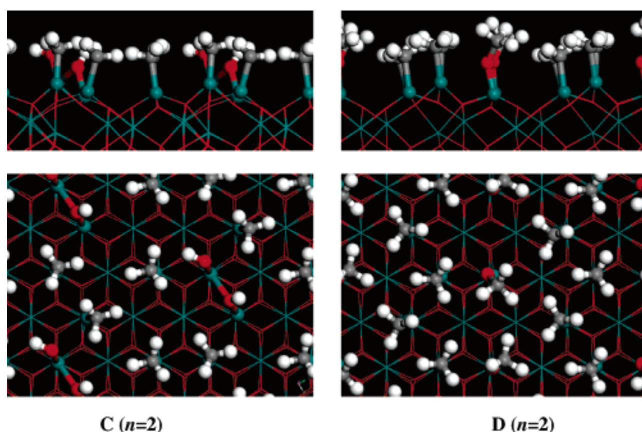

Figure 7. Models for products of oxidation by ozone. Left: Partially hydroxylated surface (**C**) $Al_2(CH_3)_4(OH)_2$, which is the proposed product after reaction with $n = 2$ oxygens per cell and desorption of C_2H_4. Right: Product (**D**) $Al_2(CH_3)_4(OCH_3)_2$, where O is trapped as methoxy and no fragments desorb; also illustrated for $n = 2$.

more highly oxidized products such as CO_2. The computed thermodynamics show that desorption of $2C_2H_4$ is energetically favored over the equivalent desorption of $CO_2 + H_2O$ by more than 250 kJ/mol (E, Table 2), probably because of the greater number of Al−O generated in the former. In addition, the C_2H_4 pathway is many times more efficient than the alternative pathways at converting the methylated surface into a hydroxylated one, and so may be expected to contribute more to the overall ALD reaction cycle. However, it will be necessary to compute activation energies in order to definitively determine which reaction pathway predominates.

Surface Al and surface OH are not observed to react with $O(^1D)$ in any of our simulations. As will be discussed below (section 4.2), this has important consequences for the quality of O_3-deposited films.

As an aside, we note that all volatile products will be oxidized to $CO_2 + H_2O$ by the plentiful O_3 in the gas phase during that pulse. However, because this does not happen at the surface, it has no bearing on the ALD chemistry. The exception is in confined geometries at low temperatures, where H_2O product may persist long enough during the O_3 pulse to adsorb and cause TMA + H_2O type reactions.

Computed H_2O desorption energetics (F, Table 2) confirm that eq 4 is endoergic and reveal a dependence on the degree of surface hydroxylation. Complete dehydration costs $\Delta E = +139$ kJ/mol H_2O at a coverage $\theta(OH) = 2.5$ H/nm^2 ($n = 2$) and $\Delta E = +193$ kJ/mol H_2O at $\theta(OH) = 5.0$ H/nm^2 ($n = 4$). Because the reaction is favored entropically, it shows strong temperature dependence, with implications for growth rate and film morphology (see section 4.1).

4. Discussion

4.1. Discussion of Growth Rate. We confirm the results of previous ALD experiments[18] that show that the deposition rate of Al_2O_3 from TMA + H_2O precursors decreases with increasing T_g (Figures 2a and 3). This decrease in growth rate can be correlated with the gradual decrease in equilibrium coverage of hydroxyl protons, $\theta_{sat}(H)$, with increasing T_g.[48] During the TMA pulse, protons can eliminate CH_4 from the surface, relieve steric crowding, and allow more TMA to adsorb. The ALD growth rate is therefore lowered by association of surface OH into H_2O followed by thermal desorption (eq 4), especially during the purge preceding the TMA pulse.

This is illustrated quantitatively by the reaction portraits[45] in Figure 8. These show how the coverage of surface intermediates varies during one ALD cycle. The saturating coverage of CH_3 at the end of the TMA pulse + purge is $\theta_{sat}(C)$, which we assume is achieved at all temperatures in both H_2O and O_3 processes. The saturating coverage of hydroxyl protons at the end of the oxygen pulse + purge is $\theta_{sat}(H)$, which is temperature-dependent. Diagonal lines at 45° ($-x$, $-y$) represent the simultaneous desorption of surf-C and surf-H as CH_4. Joining the lines into a cycle then dictates the shape of the reaction portrait. The amount of CH_4 desorbed per unit surface area in one cycle is simply the sum of the saturating coverages, $\theta_{sat}(C) + \theta_{sat}(H)$. CH_4 desorption and Al_2O_3 growth are related (by eq 1 for TMA + H_2O), so the rate of Al_2O_3 deposition is $[\theta_{sat}(C) + \theta_{sat}(H)]/6$ per cycle. This is expected to decrease linearly with decreasing $\theta_{sat}(H)$, i.e., as T_g increases. As an illustration, consider typical experimental values[46] at 200 °C of $\theta_{sat}(C) = 5.1$ atoms/nm^2 and $\theta_{sat}(H) = 8.7$ atoms/nm^2, which give an ideal growth rate of 2.3 Al_2O_3/nm^2 per cycle, or half a monolayer per cycle. This is a plausible ideal value, 9% higher than the measured rate (Figure 3).

For the O_3 process, when the thickness increment per cycle is normalized to take density differences into account, we see a decrease in growth rate with increasing T_g that is more pronounced than for H_2O (Figure 3). Such a decrease is surprising, because O_3 dissociation into reactive O radicals

(45) Elliott, S. D. *Comput. Mater. Sci.* **2005**, *33*, 20−25.
(46) Puurunen, R. L.; Lindblad, M.; Root, A.; Krause, A. O. I. *Phys. Chem. Chem. Phys.* **2001**, *3*, 1093−1102.
(47) Niinistö, L.; Päiväsaari, J.; Niinisto, J.; Putkonen, M.; Nieminen, M. *Phys. Status Solidi A* **2004**, *201*, 1443−1452.
(48) Kim, Y. B.; Tuominen, M.; Raaijmakers, I.; de Blank, R.; Wilhelm, R.; Haukka, S. *Electrochem. Solid State Lett.* **2000**, *3*, 346−349.

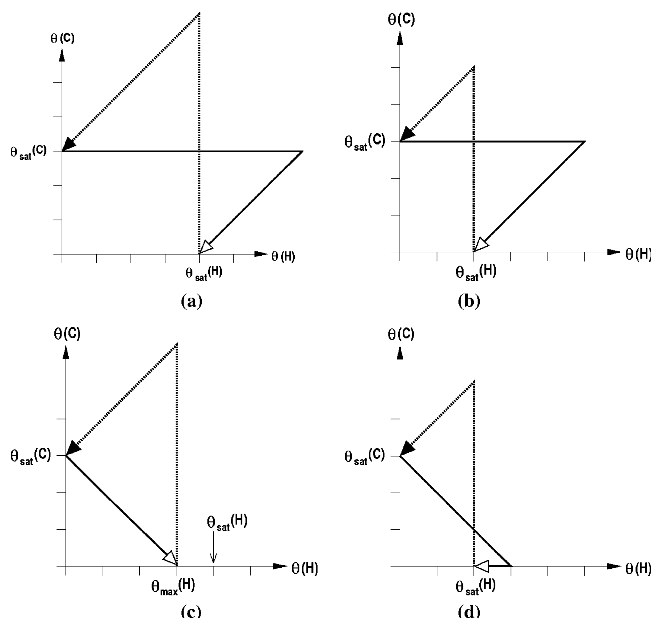

Figure 8. Reaction portraits[45] for ALD using TMA + H_2O at (a) low and (b) high temperatures and for TMA + O_3 at (c) low and (d) high T_g. The space shows coverages of intermediates at the growing surface; H coverage (as surf-OH) on the *x* axis and C coverage (as surf-CH_3) on the *y* axis. Typical units are atoms/nm^2 or μmol/m^2. The TMA pulse and purge is a dotted line, and the oxygen precursor pulse and purge is the solid line. Horizontal lines represent H_2O adsorption (+*x*) or desorption (−*x*), vertical lines (+*y*) represent TMA adsorption, and diagonals represent the desorption of CH_4 (−*x*, −*y*) or C_2H_4 (+*x*, −*y*).

is expected to be more efficient at 300 °C than at 150 °C,[23] so that elimination of ligands from the surface by O radicals would be expected to be enhanced at higher T_g. Clearly, the action of O radicals is not rate limiting. Instead, we suggest that surface OH introduces the temperature dependence (see below).

Following published TOF-SIMS results,[13] we assume that the TMA pulse proceeds identically in the H_2O and O_3 cases, with the same $\theta_{sat}(C)$. Over the T_g of interest, $\theta_{sat}(C)$ is temperature-independent.[18] In addition, at a given T_g, the maximum $\theta_{sat}(H)$ that can be achieved must be the same in both processes. Whether the product is C_2H_4 or CO_2, both mechanisms investigated above for the reaction of O_3 (section 3.2) involve surface CH_3 being replaced by surface OH; the loss of surf-C along with the gain of surf-OH is represented by a 45° diagonal line (+*x*, −*y*). We thus construct reaction portraits for TMA + O_3 ALD that show C fragments being eliminated and OH being regenerated during the O_3 pulse (panels c and d of Figure 8).

Depending on $\theta_{sat}(H)$, two shapes of reaction portrait are possible. First, if $\theta_{sat}(H) \geq \theta_{sat}(C)$, insufficient surface OH is generated by the oxidation of CH_3 to saturate the surface and $\theta_{max}(H) = \theta_{sat}(C)$. Again, the Al_2O_3 growth rate can be determined from the changes in C or H coverage in one cycle. This means that the growth rate in terms of Al_2O_3 units is $[\theta_{sat}(C) + \theta_{max}(H)]/6 = [2\theta_{sat}(C)]/6$ per cycle, which is independent of T_g (Figure 8c). This would account for the lower growth rate of the O_3 process relative to that of H_2O, but not for the marked T_g dependence observed in our experiments. We can speculate that such temperature-independent growth may be possible for TMA + O_3 at even lower temperatures (T_g < 150 °C). There are reports of temperature windows at which growth is constant for ozone ALD,[47] for example, with various Zr precursors.[6]

A second possibility is that $\theta_{sat}(H) < \theta_{sat}(C)$. In this case, oxidation produces excess surface OH and associative desorption of H_2O can occur (eq 4). As a result, the dependence on T_g is more like that of H_2O ALD, with a growth rate of $[\theta_{sat}(C) + \theta_{sat}(H)]/6$ Al_2O_3 per unit surface area per cycle (Figure 8d). On the basis of the measured decrease of rate with T_g for TMA + O_3 (Figure 3), we can conclude that this second case applies over the temperature range 150−300 °C. H_2O is therefore a product during the O_3 pulse and the amount of H_2O evolved increases with T_g. This means that substantial surface OH is produced by the action of O_3 on adsorbed organic fragments. Combining this with the ab initio evidence for C_2H_4 as a product (section 3.2), we propose the following reactions for TMA+O_3 ALD.

TMA half reactions:

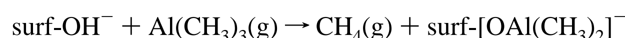

$$\text{surf-OH}^- + Al(CH_3)_3(g) \rightarrow CH_4(g) + \text{surf-}[OAl(CH_3)_2]^-$$

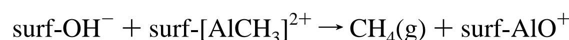

$$\text{surf-OH}^- + \text{surf-}[AlCH_3]^{2+} \rightarrow CH_4(g) + \text{surf-AlO}^+$$

O_3 half reactions:

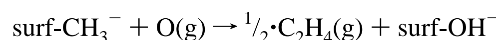

$$\text{surf-CH}_3{}^- + O(g) \rightarrow {}^1/_2 \cdot C_2H_4(g) + \text{surf-OH}^-$$

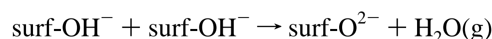

$$\text{surf-OH}^- + \text{surf-OH}^- \rightarrow \text{surf-O}^{2-} + H_2O(g)$$

The relative importance of these half reactions is determined by the values of $\theta_{sat}(C)$ and $\theta_{sat}(H)$, as illustrated in Figure 8. We therefore define one variable $x = [\theta_{sat}(C) - \theta_{sat}(H)]/[\theta_{sat}(C) + \theta_{sat}(H)]$, so that $0 \leq x \leq 1$, and this quantifies the relative occurrence of H_2O desorption within the ALD cycle. The half reactions thus combine to an overall ALD reaction

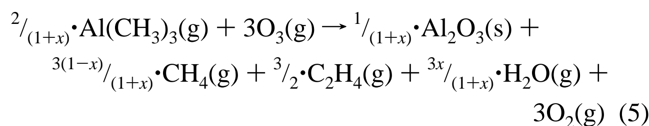

$$^2/_{(1+x)} \cdot Al(CH_3)_3(g) + 3O_3(g) \rightarrow {}^1/_{(1+x)} \cdot Al_2O_3(s) + {}^{3(1-x)}/_{(1+x)} \cdot CH_4(g) + {}^3/_2 \cdot C_2H_4(g) + {}^{3x}/_{(1+x)} \cdot H_2O(g) + 3O_2(g) \quad (5)$$

This equation assumes the same $\theta_{sat}(C)$ as eq 1. It is therefore clear that the overall growth rate scales as $^1/_{(1+x)}$ as the temperature (and *x*) is increased, relative to the low-temperature growth rate ($\theta_{sat}(H) \geq \theta_{sat}(C)$, $x = 0$, relative rate = 1). At very high temperatures, there would be no surface OH ($\theta_{sat}(H) = 0$, $x = 1$), and the growth rate would have dropped by half.

Figure 3 shows that using O_3 as an oxygen source in our growth experiments yields molar growth rates that are up to 15% lower than those for the corresponding H_2O process at a given T_g, and a similar difference in rates is reported at 400 °C.[12] As discussed below (section 4.2), we suggest that this is due to suboptimal coverage of CH_3 groups during the TMA pulse, which in turn is due to an inhomogeneous OH distribution from the action of O_3.

Considering other precursors for the ALD of metal oxides, it is clear that the above discussion of temperature dependence applies only when surface OH is the product of metal-precursor oxidation. As a counterexample, we point out that the Hf precursor $HfCl_4$ contains no oxidizable H, and we

have found that the rate of $HfCl_4 + O_3$ ALD in fact increases (not decreases) with T_g (from 0.04 nm/cycle at $T_g = 200$ °C to 0.09 nm/cycle at $T_g = 350$ °C).

4.2. Discussion of Film Electronic Density and Morphology. Over the range of temperatures considered here (150−300 °C), the TMA + H_2O ALD process yields remarkably consistent Al_2O_3 films. There is a slight decrease in density and increase in roughness with increasing T_g, but overall the process is nearly temperature-independent when H_2O is used. By contrast, the films deposited using O_3 as the oxygen source exhibit an electronic density (Figure 2b) that increases with T_g from a low value at 150 °C to a value matching that of the H_2O process at 300 °C. The low density of the films deposited using O_3 at low T_g can mean that the layer is composed of (i) Al_2O_3 + voids, (ii) nonstoichiometric Al_xO_y, (iii) Al_2O_3 + low-density elements (C, F), or a combination of all three possibilities. Combined TEM, ESI, and TOF-SIMS analyses on films a and b (Figure 4) suggest that hypothesis (i) is very likely the correct one. The fact that the films from the O_3 process are consistently rougher than their H_2O counterparts at all temperatures (Figure 5) also points to void formation. F is not detected in films a and b. Hypothesis (ii) is weak because, from the compositional analysis reported in ref 17, strongly substoichiometric oxides such as AlO and Al_2O are not expected to form at $T_g = 150$ °C. Moreover, other nonstoichiometric Al oxides have electronic densities not significantly different from that of Al_2O_3 (corundum phase = 1.19 e$^-$/Å^3, and gamma phase = 1.07 e/Å^3); for example, $Al_{2.144}O_{3.20}$ has an electronic density of 1.09 e$^-$/ Å^3.[26] Therefore, not only can XRR analysis not discriminate between the various nonstoichiometric phases but also these cannot significantly lower the electronic density to the values detected for film b. We note in passing that these hypotheses do not suggest a reason for the peak in surface roughness for deposition at $T_g = 250$ °C (films e and f) that we observe. We now proceed to discuss what aspects of the O_3 deposition mechanism can lead to void formation.

We suggest that the poor film morphology of all the films deposited using O_3 as the oxygen source can be traced to an inhomogeneous distribution of hydroxyl protons on the surface at the start of the TMA pulse. The ideal operation of the TMA pulse is dependent on the availability of surface protons for reaction with adsorbing $Al(CH_3)_3$, so that CH_4 is produced and the $Al(CH_3)_2$ or $Al(CH_3)$ fragment becomes anchored to the surface.[20] An uneven distribution of immobile protons therefore leads to an uneven distribution of surface $Al(CH_3)_x$ and suboptimal saturation [θ_{sat}(C)], if we assume that these adsorbates are likewise immobile at low temperatures. A direct consequence of suboptimal θ_{sat}(C) is a lower growth rate (section 4.1). In addition, as the ALD cycle proceeds, the action of O_3 regenerates protons at the same site, frozen in an uneven distribution, which then undergo no further reaction with gas-phase O_3. Over many cycles, the mode of film deposition will therefore resemble island growth and will result in a rough, porous, low-density film.

The effect should become less marked as T_g is raised, because protons become more mobile and more evenly distributed over the surface. Such annealing accounts for the increase in density with T_g that we observe for O_3-derived films (Figure 2). The measured roughness (Figure 5) increases slightly with T_g, which may indicate that the evolution of roughness with T_g is complicated by the concomitant decrease in surface coverage of protons.

We suggest that the effect of frozen protons is absent when H_2O is used as a precursor, regardless of T_g, because continuous exchange of H_2O between the surface and the gas phase during that pulse will ensure a stable, evenly distributed coverage of hydroxyl protons. Although no net reaction may occur, this dynamic equilibrium between oxide, hydroxide, and vapor may act to eliminate irregularities in surface morphology and thus densify the film. We propose this as the reason for the broadly T_g-independent morphology of the films deposited by TMA + H_2O and for their low roughness. This is consistent with slow desorption of H_2O during the purge, as inferred from rate studies.[19] (It may be that a similar argument can account for the excellent conformality of ALD films, but we do not present conformality data here).

The 3.8−3.9 nm thick oxygen-rich IL found at the bottom of film a (deposited using H_2O at 150 °C) might explain the lack of adhesion of this film on Si(100). Such a thick IL is not found in Al_2O_3 films deposited at higher T_g or in those deposited using O_3 as the oxygen source. Therefore, the thick oxygen-rich IL is likely to result from the high surface OH coverage at low T_g,[48] together with continuous exchange of H_2O between the surface and the gas phase during the H_2O pulse. We suggest that this leads to mixing of Si−OH and Al−OH in the growing film, both of which are reactive with respect to TMA fragments. At higher temperatures, similar mixing may lead to Al−Al bonds and Si oxidation, as reported for films deposited at 350−400 °C.[11] We point out that lack of adhesion to Si of films deposited using H_2O as the oxygen source at low T_g seems to be a general property; indeed, we found the problem also for films deposited at 150 °C from $HfCl_4 + H_2O$ and $ZrCl_4 + H_2O$.

5. Conclusion

We present a systematic study of the dependence of deposition rate and morphology of Al_2O_3 films on temperature over the range T_g = 150−300 °C for two ALD processes, TMA + H_2O and TMA + O_3. The films were characterized using XRR, TEM/ESI, and TOF-SIMS. In the case of both oxygen precursors, the molar growth rate per cycle decreases with increasing T_g, and at no temperature does the O_3 process yield faster growth than the H_2O process.

To investigate the surface chemistry controlling the growth, we performed ab initio slab calculations on the reactions of O atoms with a methylated surface. The fundamental redox reaction is the transfer of hydride (H^-) from organic fragments on the surface to adsorbing O atoms, which regenerates surface hydroxyl (OH^-) and produces volatile molecules such as C_2H_4. Such reactions are likely to contribute more to film growth than continued oxidation at the surface to $CO_2 + H_2O$. Therefore, both types of oxygen source (H_2O and O_3) lead to a coverage of surface hydroxyl, and the decrease of growth rate with T_g in both processes

can be correlated with the decrease in hydroxyl coverage as the temperature is elevated and H_2O desorbs.

However, use of O_3 as oxygen source yields thicker films at low T_g, because of their lower density, correlated with the existence of voids in the alumina layers. We suggest that low density and void formation can be attributed to an inhomogeneous distribution of immobile protons at the growing surface in these cases, leading to uneven growth. By contrast, treatment of the growing surface with excess H_2O in the TMA + H_2O process ensures homogeneous surface OH, a denser and smoother film, and a slightly higher growth rate, regardless of T_g. However, at low T_g, the interaction of H_2O with Si seems to produce a thicker oxygen-rich interfacial layer, which adheres poorly to the Si substrate.

We have thus observed and accounted for variations in the growth mechanism with oxygen source and temperature and have examined the consequent variations in film morphology. These mechanistic insights into TMA + O_3 ALD may also be relevant for ALD processes for which oxygen plasma is used as a precursor.

Acknowledgment. The authors thank Dr. K. Kukli (Universities of Tartu and Helsinki) for valuable discussions. Dr. M. Perego (MDM) is acknowledged for TOF-SIMS measurements of some of the samples studied in this work. S.D.E. acknowledges funding from the European Community under the “Information Society Technologies” program through the HIKE project http://www.tyndall.ie/hike.

CM0608903